Synthesis and Characterization of Polybenzimidazole–Nanodiamond Hybrids via *In Situ* Polymerization Method

Ru Zhang, ZhiXing Shi, Yang Liu, Jie Yin

School of Chemistry and Chemical Engineering, State Key Laboratory for Metal Matrix Composite Materials Shanghai Jiao Tong University, Shanghai 200240, People's Republic of China

Received 22 July 2011; accepted 15 November 2011
DOI 10.1002/app.36497
Published online 1 February 2012 in Wiley Online Library (wileyonlinelibrary.com).

ABSTRACT: Poly[2,2′-(*p*-oxydiphenylene)-5,5′-bibenzimidazole] (OPBI) was polymerized in poly(phosphoric acid) (PPA) with the presence of the pristine nanodiamonds (NDs) (0.2–5 wt %) to fabricate NDs-*g*-OPBI/OPBI nanocomposites via Friedel–Crafts (F-C) reaction. The OPBI chains were successfully attached to the NDs through F-C reaction between carboxylic acid from OPBI and NDs, which was proved by nuclear magnetic resonance, X-ray photoelectron, and X-ray diffraction. NDs-*g*-OPBI/OPBI nanocomposites show more homogeneous dispersion than the physical blending containing pristine NDs and OPBI matrix, as showed through scanning electronic microscopy images. The mechanical properties, including Young's modulus, yield strength, and tensile strength are all improved by the introduction of NDs (<1 wt %) without loss of ductility, which overcomes the brittleness brought by the addition of inorganic reinforced agent in traditional composites. Dynamic mechanical analysis results showed that the modulus of the ND-*g*-OPBI/OPBI nanocomposites was significantly higher than OPBI matrix, and the NDs-*g*-OPBI/OPBI nanocomposites displayed more pronounced improvement than the physical blending, which could be ascribed to the homogeneous dispersion of NDs particles and the covalent bonding between NDs and OPBI via F-C reaction. Thermogravimetric analysis indicated that all the OPBI nanocomposites containing NDs displayed the improved thermal stability. © 2012 Wiley Periodicals, Inc. J Appl Polym Sci 125: 3191–3199, 2012

Key words: polymer synthesis and characterization; mechanical properties; thermal properties; modification; membranes

INTRODUCTION

Incorporating inorganic agents into polymers matrix to improve the properties of polymers continues to be a driving force for the development of new composites materials.[1–6] The nanoscaled distribution of reinforcing agents into the polymer matrix can optimize the intercomponent interactions and affords the materials with improved properties. In recent years, polymer blends containing dispersed nanodiamond (ND) represent a new class of materials with a combination of interesting properties generally not obtained in conventional polymers.[7–10] Though remarkable efforts have been paid to polymer nanocomposites, the research on diamond-filled polymer composites is still very limited.[11–13]

ND got more and more attention until two landmark articles were published in 1988.[14,15] It has many beneficial properties, such as chemical inertness of the core, interesting electronic and mechanical properties, the stability of luminescent, lattice defects, and other characteristics, making nanoscale diamond an ideal material for many fields.[16] ND can be used as abrasives for the semiconductor and optical industries, additives to lubricants for engines and moving gears, protein adsorbents, and even medicinal drugs, also used for extra durable and hard coatings and polymer reinforcements.[17–19] Several kinds of ND-based nanoelements are readily fabricated including surface-modified ND which promotes crosslinking with polymer chains during nanocomposite curing,[20–22] synthesized NDs polymer brushes using atom transfer radical polymerization,[23] oxidation,[24] fluorination,[25,26] as well as ultraviolet irradiation[27] and NDs platform for gene delivery,[28,29] which represent a new generation of polymeric materials lying at the interface of organic and inorganic materials.

Polybenzimidazole (PBI) is a kind of aromatic heterocyclic polymers containing benzimidazole units. It was initially developed by Celanese as a fire-resistant fiber.[30] PBI molecules are characterized by their high thermal, physical, and chemical stabilities, mainly due to their rigid structures.[31] Owing to its excellent chemical and thermal stabilities, PBI is widely used in firefighters' protective clothing,[32] high-temperature gloves,[33] astronaut flight suits, ultrafilters,[34] and other type of separatory media. In addition, PBI is one of the most studied materials

Correspondence to: Z. Shi (zxshi@sjtu.edu.cn).

for application in proton exchange membrane fuel cell. Acid doping in PBIs often results in an increase both in their proton conductivities and thermal stability.[35,36] To improve the mechanical properties of PBI, several kinds of inorganic fillers such as montmorillonite, etc., have been incorporated into the PBI matrix, but the reinforcement effect is not satisfactory.[37] Inspired by the method for the modification of NDs based on Friedel–Crafts (F-C) reaction using poly(phosphoric acid) (PPA/P_2O_5) as solvents proposed by Tan research group,[38] we wonder whether the ND with proper size can be incorporated to PBI to prepare NDs-reinforced PBI.

Recently, our research group has successfully prepared the soluble poly[2,2′-(*p*-oxydiphenylene)-5,5′-bibenzimidazole] (OPBI) in PPA/P_2O_5 (a kind of mild protonated acid).[39] Good solubility of such polymers in high polar solvent makes it a potential candidate suitable for the preparation of NDs/OPBI polymers in one-pot synthesis, where F-C reaction of OPBI and NDs and polymerization could be combined together to be carried out simultaneously in one pot. In this article, we reported that PBI act as an excellent NDs' dispersant and described the fabrication of novel polymer nanocomposites composed of PBI and NDs. To the best of our knowledge, there has been no precedent report on NDs/OPBI nanocomposites based on this novel method. Here, we reported the preparation of NDs/OPBI nanocomposites, where NDs were incorporated into polymer via the formation of covalent bonds using the PPA/P_2O_5 as medium. For comparison, the NDs/OPBI hybrids via a physical blending were also obtained. The morphological and thermomechanical properties of two types of organic–inorganic hybrid composites were comparatively investigated based on nuclear magnetic resonance (NMR), tensile test, scanning electronic microscopy (SEM), X-ray diffraction (XRD), dynamic mechanical analysis (DMA), and thermogravimetric analysis (TGA).

EXPERIMENTAL

Materials

NDs were purchased from Diamond Source. 3,3′-Diaminobenzidine (DABz) was purchased from J&K Chemical in Shanghai and used without further purification. 4,4′-Dicarboxydiphenyl ether (DCDPE) was supplied by Peakchem (Shanghai) and vacuum dried at 80°C before use. Phosphorus pentoxide, PPA, and dimethyl sulfoxide (DMSO) were purchased from Sinopharm Chemical Reagent (SCRC). DMSO was distilled under reduced pressure and dried over 4 Å molecular sieves before use. Other materials were used as received.

Measurements

^{1}H-NMR spectra were recorded on a Varian Mercury Plus 400 MHZ instrument. SEM was used to observe the phase structure of ND-containing OPBI hybrids, all specimens were examined with a Hitachi S210 SEM at an activation voltage of 25 KV. The morphology of the cry-fractured surface of composite was obtained using FE-SEM (JSM-7401 F, JEOL, Japan). XRD spectra were acquired by D/max-2200/PC (Japan Rigaku Corporation) using Cu Kα radiation. X-Ray photoelectron (XPS) spectra were recorded on an ESCALAB 250 spectrometer (VG scientific) with an Alka radiation (1486.6 eV). The dynamic mechanical tests were carried out on a dynamic mechanical thermal analyzer (MKIII, Reometric Scientific, United Kingdom) with the temperature rang from 100 to 400°C. The frequency used is 1.0 Hz and heating rate 10°C/min. TGA was performed in nitrogen with a Perkin-Elmer TGA 2050 instrument at a hearting rate of 20°C/min. For each measurement, the sample cell was maintained at 100°C for 30 min to evaporate the absorbed water in the sample before test. Tensile measurements were performed with an Instron 4465 instrument in ambient atmosphere at a crosshead speed of 5 mm/min.

Polymerization of NDs-g-OPBI/OPBI nanocomposites

To a 100-mL dry three-neck flask equipped with a mechanical stirring device, 45 g of PPA and 4.5 g of phosphorus pentoxide were added under nitrogen flow. The mixture was heated and stirred until phosphorus pentoxide was completely dissolved. After cooling to room temperature, 1.0713 g (0.5 mmol) of DABz, 1.2912 g (0.5 mmol) of DCDPE and different amounts of NDs (0.2, 0.5, 1, and 5 wt %) were added to the reaction flask. The reaction mixture was stirred and heated at 150°C for 4 h and 190°C for 20 h, respectively. On cooling, the gel-like mixture was transferred to ice water with stirring, and the precipitate was filtered off. The solid was soaked in 5% sodium bicarbonate solution for 2 days, then filtered, thoroughly washed with deionized water and dried in vacuum at 120°C for 10 h.

For comparison, OPBI was prepared without adding NDs in the same procedure as above. The silk like product was brown, and the yield was about 96% (2.268 g).

Preparation of ND-blending OPBI hybrids

To a 50-mL dry two-neck flask, 10 mL DMSO and different amounts of NDs (0.2, 0.5, 1, and 5 wt %) were added. The mixture was magnetically stirred under nitrogen flow in an ultrasonic bath for 1 h, and then OPBI was added into the flask. The

mixture was magnetically stirred at 80°C for 12 h until the OPBI was completely dissolved in DMSO. On cooling, the mixture was transferred to ice water with stirring, and the precipitate was filtered off. The solid was thoroughly washed with deionized water and dried in vacuum at 120°C for 10 h.

Preparation of NDs-g-OPBI

To make sure OPBI had really grafted from NDs, Soxhlet extraction was utilized to prepare NDs-*g*-OPBI. NDs-*g*-OPBI/OPBI nanocomposite was treated with DMSO in Soxhlet extractor for 5 days to get rid of noncovalent OPBI. The resultant product was subsequently characterized by NMR, Raman spectroscopy, XRD, and XPS.

Membrane formation

Polymer solution of 5–10 wt % in DMSO was sonicated for 15 min, and then casted onto glass plates and dried in an air oven at 80°C for 5 h. The films were peeled off from glass plate and dried in vacuum at 120°C for 10 h, followed by washing in water at 60°C for 12 h to remove the residue solvent.

RESULTS AND DISCUSSION

Interaction between NDs and OPBI based on F-C reaction

^{1}H-NMR

Proton NMR spectra of NDs, OPBI, and NDs-*g*-OPBI in deuterated DMSO are shown in Figure 1. Although NDs can be dispersed into DMSO to form a homogeneous suspension, no peak was detected in its ^{1}H spectrum [Fig. 1(a)]. However, ^{1}H spectrum could detect the peak for the ND-*g*-OPBI, which shows a good solubility of ND-*g*-OPBI in DMSO. Resonances observed at 7.31, 7.56, 7.75, and 8.26 ppm for the NDs-*g*-OPBI [Fig. 1(c)] are readily assigned to the corresponding resonances of the neat OPBI. Unlike the considerable signal broadening observed in polymer/multi-wall nanotubes systems,[40,41] very little relaxation broadening was observed for NDs-*g*-OPBI. Similar results are also found in ND particles modified by poly(ether-ketone).[42] All these observations indicated a successful grafting of OPBI chains onto NDs via F-C reaction.

XPS

In addition, XPS was utilized to individually elucidate the compositions of the NDs and NDs-*g*-OPBI. In each case, an initial broad scan was performed (800–0 eV) to establish the gross element composition of the surface of the sample. Both the NDs and NDs-*g*-OPBI show peaks at 285 and 533 eV, which are the characteristic peaks of C1s and O1s, respectively. However, after the graft of the OPBI molecules, the spectrum for NDs-*g*-OPBI exhibited an additional new peak at 401 eV for N1s as compared to NDs. The N1s peak came from the imidazole group of the OPBI,[43] revealing the successful graft of OPBI chains to NDs.

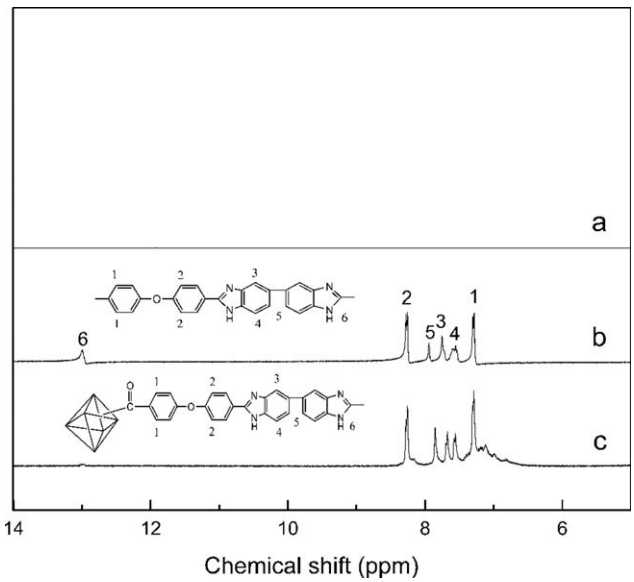

Figure 1 ^{1}H-NMR spectra of (a) NDs, (b) OPBI, and (c) NDs-*g*-OPBI.

Furthermore, clear evidence that the NDs have been chemically modified was provided by the detailed analysis for C1s in the XPS spectra. Both pristine NDs [Fig. 2(c)] and NDs-*g*-OPBI [Fig. 2(d)] display peak intensity at 284.7 and 286.1 eV, which are corresponded to C—C, C—H, and C—O species, respectively.[44] For the NDs-*g*-OPBI, the new peaks at 286.7 eV indicating that a high density of carboxyl group is produced on the surface of NDs. It can also be seen in Figure 2(d) that the existence of 285.5 eV peak is attributed to the C—N linkage. Detailed analysis of the XPS spectra provides clear evidence that the grafting of OPBI to NDs has been successfully achieved.

SEM

SEM was applied to characterize the fracture surface of composites to evaluate the dispersion of NDs in OPBI matrix. The surfaces of NDs-*g*-OPBI/OPBI [Fig. 2(b,d,f)] and NDs/OPBI [Fig. 2(c,e,g)] are distinctly different by a side-by-side comparison. For the physical blending, it is found that the fracture surfaces of the NDs/OPBI exhibit nonuniform dispersion and the tendency for agglomerates of the unmodified NDs. The phenomenon of aggregation becomes more pronounced as the content of the NDs increases. Such poor dispersion is related with the incompatibility between OPBI and NDs, leading to a limitation of stress transfer. However, the NDs-

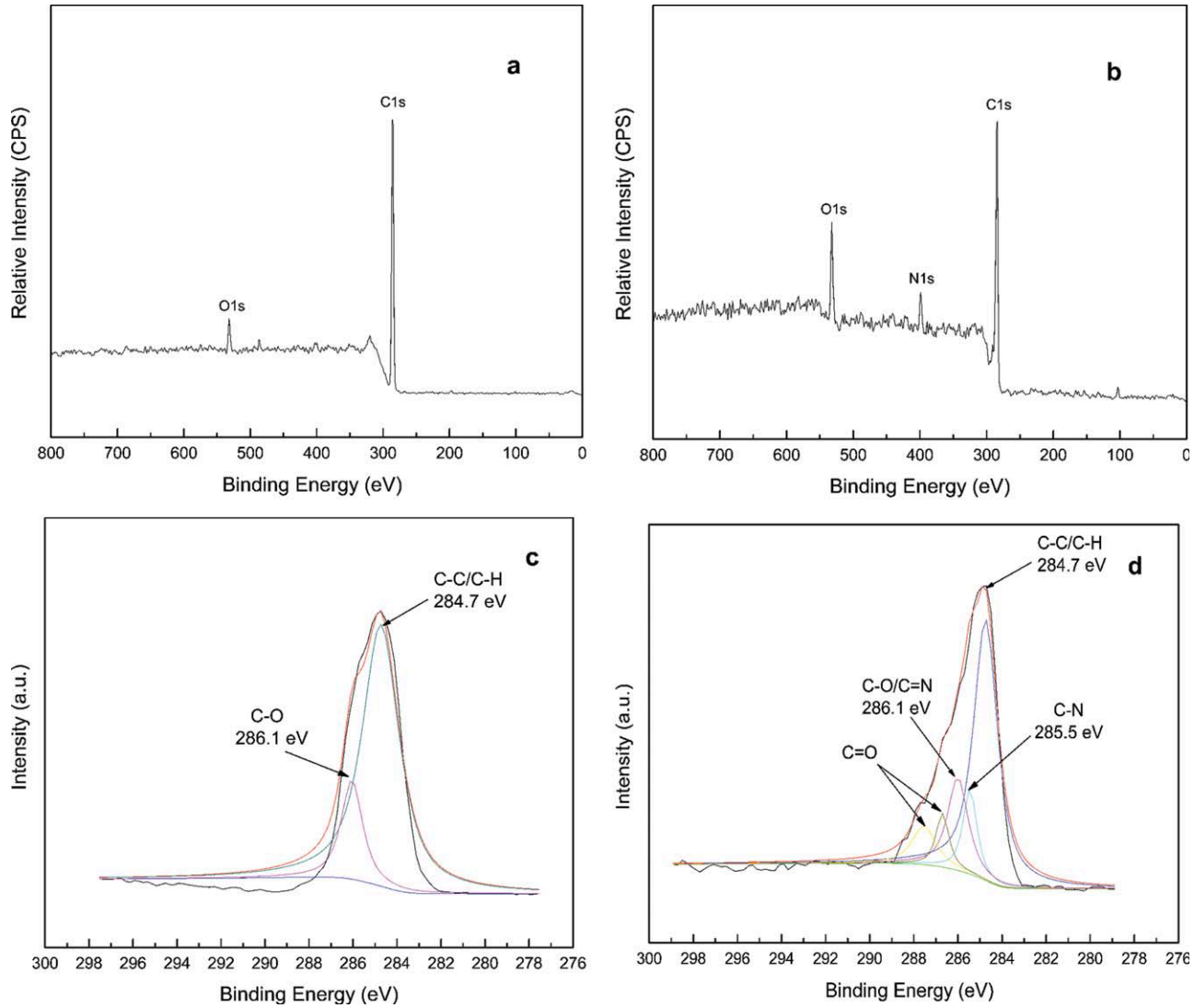

Figure 2 XPS spectra: (a) wide scan spectrum and (c) C1s narrow scan spectrum of NDs; (b) wide scan spectrum; and (d) C1s narrow scan spectrum of NDs-*g*-OPBI. [Color figure can be viewed in the online issue, which is available at wileyonlinelibrary.com.]

g-OPBI/OPBI system shows homogeneous dispersion, and it is difficult to detect NDs in the fracture surface. As the loading of NDs increases, good dispersion is still achieved and most of the NDs are embedded and tightly held to the OPBI matrix. Such good dispersion would account for different mechanical and thermal properties for these two samples as will be discussed later.[45,46]

XRD

The wide-angle X-ray diffraction (WAXRD) measurements between 2° and 80° were applied to examine the crystalline structure of nanocomposites. Figure 4 gives the WAXRD diffractograms of NDs/OPBI nanocomposites as well as ND.

NDs particles show diffraction peaks at 44.1° (equivalent to an interplanar spacing of 2.05 Å) and 75.4° (1.26 Å) in 2θ. These two characteristic diffraction peaks are attributed to the (111) and (220) plane of diamond.[47] However, these intense reflections could not be observed in NDs-*g*-OPBI/OPBI nanocomposites which contained 5 wt % NDs, indicating that NDs were dispersed in the OPBI chains without crystalline phase. On the other hand, all the WAXRDs of the OPBI films present two broad peaks from 10° to 26°, which suggests that all the OPBI films are noncrystalline.

Mechanical properties of the nanocomposites

Figure 5(a) shows the stress–strain curves of NDs-reinforced OPBI composite prepared via F-C reaction. The young's modulus, tensile strength, toughness, and ultimate strain of the composites are given in Table I. For comparison, composites of OPBI

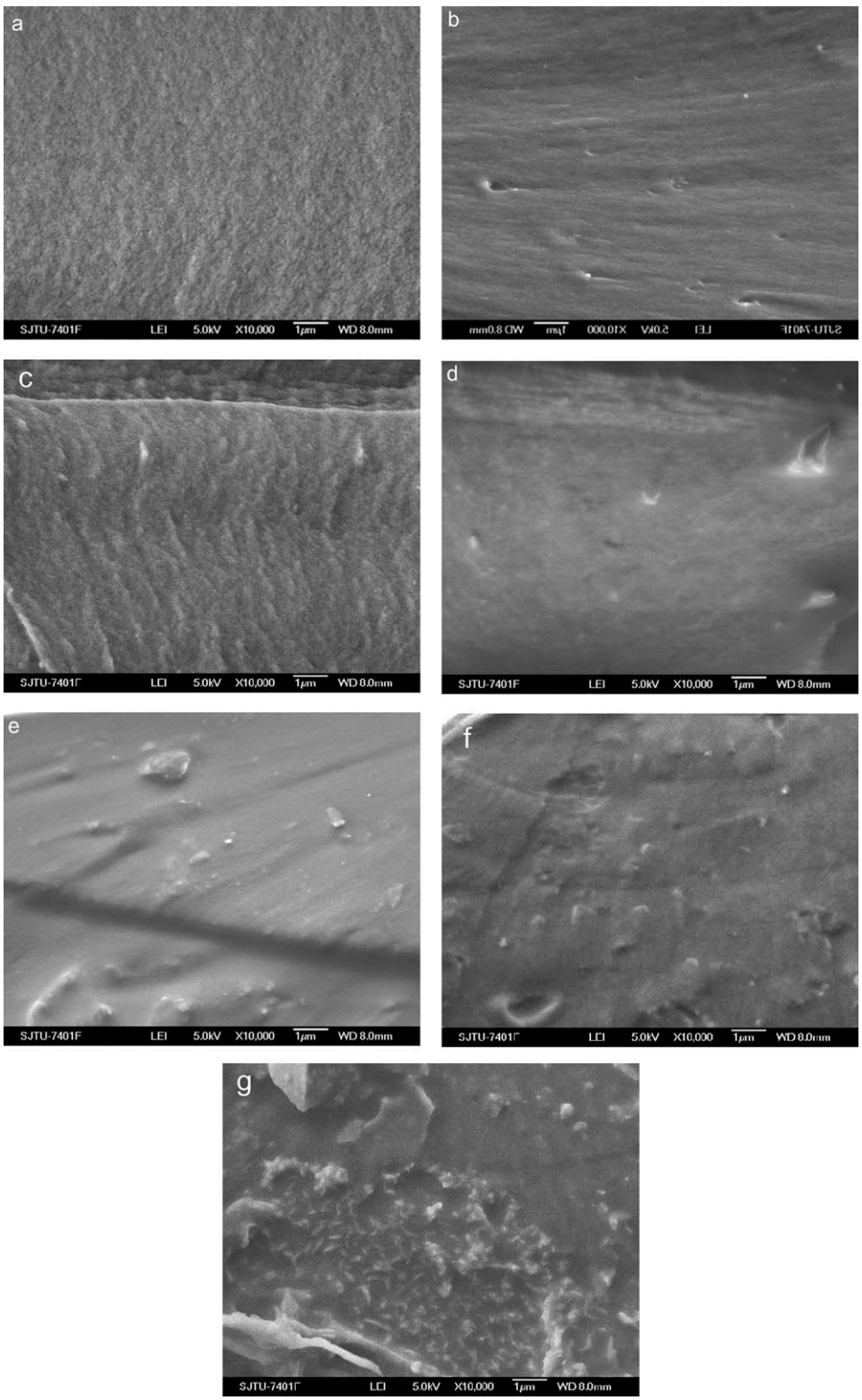

Figure 3 SEM images of fractured surface: (a) OPBI; (b), (d), and (f): 0.2, 1, 5% NDs-*g*-OPBI/OPBI; (c), (e), and (g): 0.2, 1, and 5% NDs/octaphenyl polyhedral oligomeric silsesquioxane (POSS).

reinforced with as-received NDs were also studied, and their stress–strain curves and mechanical properties are shown in Figure 5(b) and Table I. For the NDs-*g*-OPBI/OPBI system, the young's modulus, yield strength, and tensile strength were improved with the incorporation of the NDs. As NDs content is increased to 1.0 wt %, the average tensile strength is increased from 129.5 to 168.7 MPa, almost 30%

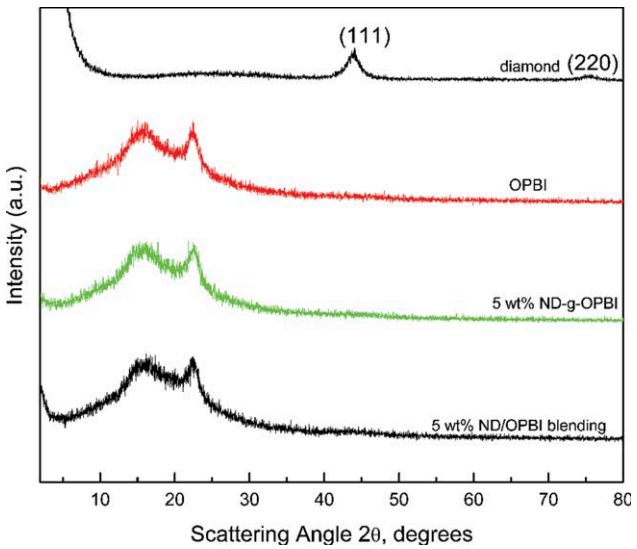

Figure 4 WAXDs of OPBI, OPBI-*g*-NDs, and OPBI/diamond nanocomposites. [Color figure can be viewed in the online issue, which is available at wileyonlinelibrary.com.]

increase, and the yield strength is also improved from 91.2 to 128.5 MPa, almost 41% improvement, compared with pristine OPBI. Also the young's modulus is increased from 2.95 to 4.01 GPa, almost 15% increase. We suppose that the presence of the strong chemical bonding formed by the reaction between the NDs-*g*-OPBI and the OPBI matrix results in good compatibility between these two phases. For as received NDs/OPBI of 1.0 wt %, the tensile strength and yield strength only slightly increases. As the loading of the raw NDs goes beyond 0.2 wt %, the yield and tensile strengths show a huge decrease. This may due to the aggregation of NDs in the OPBI matrix, and the efficient stress transfer between ND and OPBI becomes weak, so the efficiency of reinforcement reduces.

Conceptually, the ductility and toughness of inorganic–organic composites are often expected to be reduced substantially on the incorporation of inorganic fillers. However, in our hybrids prepared based on F-C reaction, the elongation of break is increased from 55.8 to 69.5% as the NDs content is increased to 0.2 wt %, which indicates that the ductility of OPBI is not compromised but improved by the addition of proper NDs content, which is quite different from the traditional composites. The improvement in ductility in the case of the compatible NDs-*g*-OPBI/OPBI nanocomposites can be attributed to the load transfer from the OPBI matrix to NDs-*g*-OPBI reinforcement via strong chemical bonding. As the addition of the ND increases to 0.5 wt %, the result for elongation of break is lower than that of the 0.2 wt % but is still higher than the OPBI matrix. For as received NDs/OPBI system, the elongation of break starts to decrease as the loading of NDs increases. In this study, NDs were tightly embedded in OPBI matrix by the covalent linkage to the OPBI via F-C reaction, and NDs act as an efficient crosslinking sites for linking the OPBI chains. As a result, the mechanical properties of OPBI were improved substantially due to a more efficient stress transfer from the matrix to NDs.

Thermomechanical properties

Shown in Figure 6(a,b) are the dynamic mechanical spectra of the NDs-*g*-OPBI/OPBI nanocomposites and the NDs/OPBI-blending hybrids, respectively. In the plots of tan δ as functional of temperature, OPBI exhibits a well-defined relaxation peak at ~ 214.4°C, which is assigned to the glass–rubber transition of the OPBI. It is seen that the T_g's of all the NDs-*g*-OPBI/OPBI nanocomposites are higher than that of the OPBI, but slightly lower than those of the

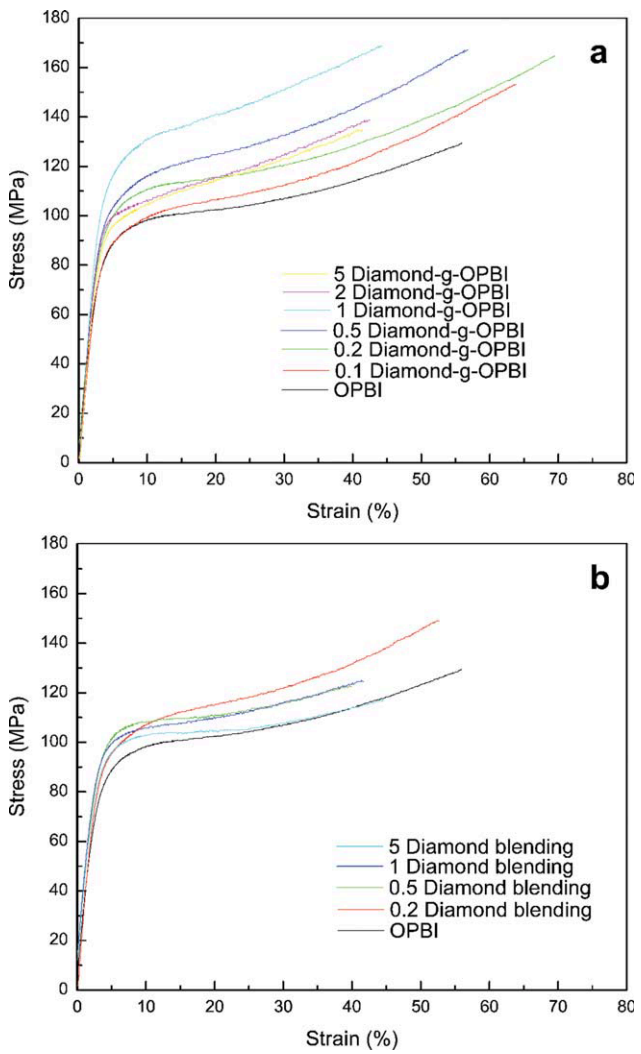

Figure 5 Selected, representative stress–strain curves: (a) NDs-*g*-OPBI/OPBI nanocomposites and (b) NDs/OPBI blending hybrids. [Color figure can be viewed in the online issue, which is available at wileyonlinelibrary.com.]

TABLE I
Mechanical Properties of the Nanocomposites

Samples	Young's Modulus (GPa)	Tensile strength (MPa)	Elongation-at-break (%)	Toughness (MPa)
OPBI	2.95 ± 0.08	129.5 ± 12.3	55.9 ± 9.1	58.6 ± 12.1
0.1% NDs-*g*-OPBI/OPBI	2.97 ± 0.11	153.2 ± 4.9	63.9 ± 4.6	73.2 ± 7.2
0.2% NDs-*g*-OPBI/OPBI	3.39 ± 0.11	164.9 ± 9.4	69.5 ± 4.7	74.9 ± 8.0
0.5% NDs-*g*-OPBI/OPBI	3.66 ± 0.22	167.2 ± 10.2	57.0 ± 4.5	73.8 ± 7.8
1% NDs-*g*-OPBI/OPBI	4.01 ± 0.15	168.7 ± 8.1	44.4 ± 5.7	61.0 ± 9.9
2% NDs-*g*-OPBI/OPBI	3.59 ± 0.19	138.6 ± 19.3	42.4 ± 8.2	48.1 ± 11.9
5% NDs-*g*-OPBI/OPBI	3.41 ± 0.10	134.8 ± 3.5	41.7 ± 2.0	45.8 ± 2.74

NDs/OPBI-blending hybrids when the content of the NDs is the same. This observation implies that the introduction of NDs reduces free volume of systems, which impedes the movement of OPBI chains.

Plots of storage modulus as functions of temperature for the OPBI and the nanocomposites with the NDs content up to 5 wt % are also shown in Figure 6. It is interesting to note that the storage modulus of all the NDs-containing composites were significantly higher than that of the OPBI. Nonetheless, it is seen that with the same content of NDs, the NDs-*g*-OPBI/OPBI nanocomposites possessed the higher storage modulus than the NDs/OPBI systems. This observation may be due to the interaction between NDs and OPBI matrix, which is associated with the dispersion of NDs particles in the OPBI matrix. For the NDs/OPBI systems, NDs were poorly dispersed in the physical blending, where the aggregation of NDs deteriorated the mechanical properties of OPBI. For the NDs-*g*-OPBI/OPBI nanocomposites, the NDs were covalently bonded to the OPBI matrix (shown in Scheme 1) via F-C reaction, and the NDs particles were homogeneously dispersed in OPBI matrix at the nanoscale. It is seen that as the NDs content is increased to 1 wt %, the storage modulus is increased from 2942.5 to 4346.1 MPa at 100°C, almost 48% increase. Therefore, the incorporation of the nanometer-sized NDs particles in the OPBI matrix brings about the significantly reinforcement for the local chain.[48]

Therefore, different dispersion states will lead to different mechanical behaviors. For the NDs-*g*-OPBI/OPBI nanocomposites prepared via F-C reaction, NDs were covalently bonded to the OPBI chain and embedded tightly into the OPBI matrix [as evidenced by Fig. 3(b,d,f)]. The strong interface interaction and good dispersion will lead to the obvious improvement in the mechanical properties of OPBI and increase in tensile strength. Such phenomenon is observed in the POSS-reinforced OPBI matrix via F-C reaction.[49]

Thermal stability

The thermal stability of the NDs-grafted OPBI composites was evaluated by TGA under nitrogen atmosphere. Figure 7 depicts the TGA curves of typical nanocomposites under nitrogen at a heating rate of 20°C/min, and the data are summarized in Table II. For the OPBI, the initial decomposition occurred at 584.7°C. However, the 5% mass loss temperature for NDs-grafted hybrids is recorded at 584.2, 591.7, 597.1, and 602.5°C for 0.2, 0.5, 1, and 5 wt % NDs, respectively. The T_d of nanocomposites is elevated

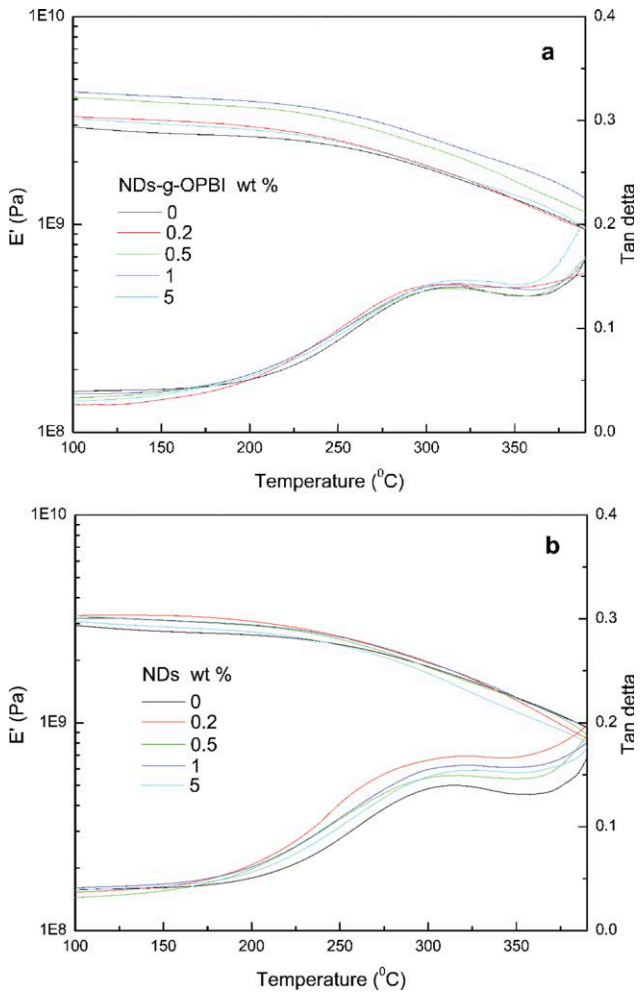

Figure 6 DMA curves: (a) NDs-*g*-OPBI/OPBI nanocomposites and (b) NDs/OPBI-blending hybrids. [Color figure can be viewed in the online issue, which is available at wileyonlinelibrary.com.]

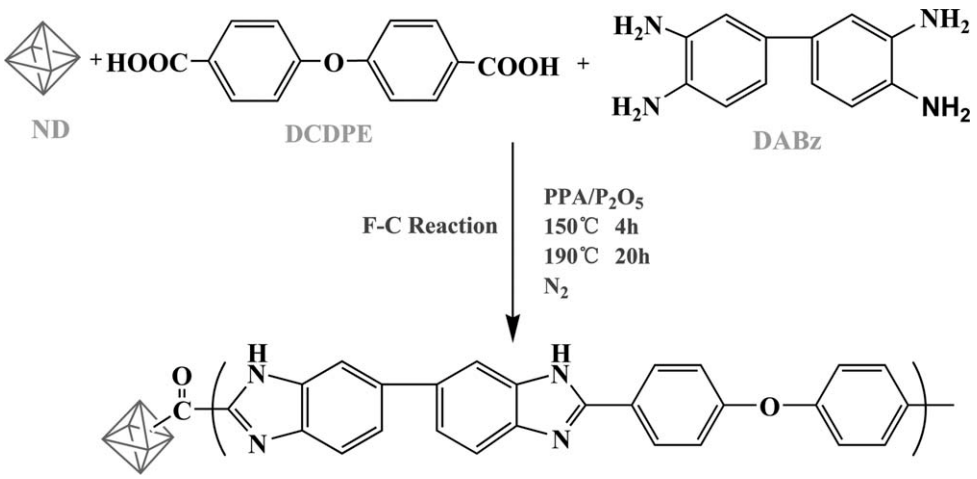

Scheme 1 Preparation of the nanocomposites containing nanodiamonds. [Color figure can be viewed in the online issue, which is available at wileyonlinelibrary.com.]

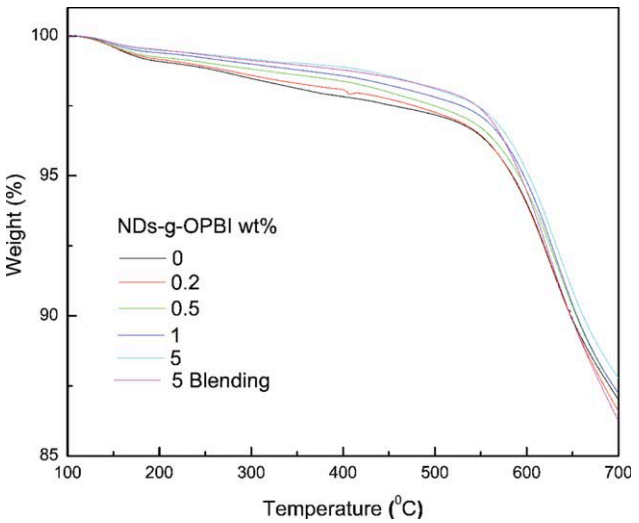

Figure 7 TGA curves of the OPBI and nanocomposites. [Color figure can be viewed in the online issue, which is available at wileyonlinelibrary.com.]

by almost 20°C at the 5 wt % loading of NDs in comparison with pure OPBI. As expected, with the same NDs content (5 wt %), the physical blending shows the lower thermal stability than those nanocomposites synthesized by F-C reaction. The enhancement of thermal stability may be attributed to the barrier effect of NDs by limiting heat transfer, which protects the underlying materials from heat attack. Simultaneously, as NDs were covalently linked with OPBI via F-C reaction, the vibration hindrance of organic segments connected covalently to NDs is also an important factor to result in the thermal improving effect.[50]

CONCLUSIONS

The NDs-containing nanocomposites of OPBI were prepared via the F-C reaction between the ND and OPBI chains. The F-C reaction, accompanied by polymerization, was started from the initially homogeneous solution of DCDPE, DABz and NDs. NMR, XPS, and XRD measurements indicate that the covalent bonding between NDs and OPBI was successfully obtained, which resulted in good dispersion of NDs in OPBI matrix as evidenced by SEM. NDs can display a highly effective reinforcement for the OPBI matrix. Both Young's modulus and tensile strength are improved by introduction of NDs (<1 wt %) without loss of ductility, which overcomes the brittleness brought by the addition of inorganic reinforced agent in traditional polymer-based composites. TGA indicates that all the OPBI nano-composites containing NDs displayed the improved thermal stability. This work provides a novel path for design and preparation of new ND hybrid materials.

TABLE II
Thermal Stability of OPBI Hybrid Composites Containing NDs

Samples	Young's Modulus (GPa)	Tensile strength (MPa)	Elongation-at-break (%)	Toughness (MPa)
OPBI	2.95 ± 0.08	129.5 ± 12.3	55.9 ± 9.1	58.6 ± 12.1
0.2% NDs blending	3.01 ± 0.13	149.1 ± 7.3	52.7 ± 3.7	62.7 ± 6.1
0.5% NDs blending	3.27 ± 0.18	123.0 ± 6.6	40.1 ± 3.1	43.0 ± 3.9
1% NDs blending	3.40 ± 0.06	125.1 ± 5.8	41.8 ± 5.2	44.9 ± 6.7
5% NDs blending	3.20 ± 0.15	116.9 ± 9.0	44.8 ± 8.6	45.7 ± 10.52

The authors thank the National Nature Science Foundation of China (No: 50973062) for the support. Additionally, the authors also acknowledge the staff of Instrumental Analysis Center of Shanghai Jiao Tong University for the measurements.

References

1. Whitesides, G. M.; Mathias, T. P.; Seto, C. T. Science 1991, 254, 1312.
2. Lan, T.; Kaviratan, P. D.; Pinnavaia, T. J. Chem Mater 1995, 7, 2144.
3. Giannelis, E. P. JOM 1992, 44, 28.
4. Theng, B. K. G. Formation and Properties of Clay–Polymer Complexes; Elsevier: Amsterdam, 1979.
5. Brinker, C.; Scherer, G. Sol-Gel Science; Academic Press:New York, 1990.
6. Theng, B. K. G. Formation and Properties of Clay–Polymer Complexes; Elsevier: Amsterdam 1979, 9.
7. Baidakova, M.; Vul, A. J Phys D: Appl Phys 2007, 40, 6300.
8. Zhang, Q. X.; Naito, K.; Tanaka, Y.; Kagawa, Y. Macromolecules 2008, 41, 536.
9. Cheng, J. L.; He, J.; Li, C. X.; Yang, Y. L. Chem Mater 2008, 20, 4224.
10. Zhang, Q. X.; Chem, M.; Lam, R.; Xu, X. Y.; Osawa, E.; Dean, H. ACS Nano 2009, 3, 2609.
11. Monteiro, S. N.; Menezes, G. W.; Rodriruez, R. J. S.; Skury, A. L. D.; Bobrovnitchii, G. S. Proceedings of the PPS 2004-Americans Regional meeting, Polymer Processing Society, Florianopolis, Brazil, 2004, p 262.
12. d'Almeida, J. A. M.; Moteiro, S. N.; Menezes, G. W.; Rodriguez, R. J. S.; Reinf, J. Plast Compos 2007, 26, 321.
13. Shenderova, O.; Tyler, T.; Cunningham, G.; Ray, M.; Walsh, J.; Casulli, M.; Hens, S.; Mcguire, G.; Kuznetsov, V.; Lipa, S. Diamond Relat Mater 2007, 16, 1213.
14. Lymkin, I.; Petrov, E. A.; Ershov, A. P.; Sakovitch, G. V.; Staver, A. M.; Titov, V. M. Dokl Akad Nauk USSR 1988, 302, 611.
15. Greiner, N. R.; Phillips, D. S.; Johnson, J. D.; Volk, F. Nature (London) 1988, 333, 440.
16. Anke, K. J Mater Chem 2011, 21, 1257.
17. Post, G.; Dolmatov, V. Y.; Marchukov, V. A.; Sushchev, V. G.; Veretennikova, M. V.; Sal'ko, A. E. Russ J Appl Chem 2002, 75, 755.
18. Bogatyreva, G. P.; Marinich, M. A.; Oleynik, N. A.; Bazaliy, G. A. In Nanostructured Materials and Coatings in Biomedical and Sensor Applications, Gogotsi Y.; Uvarova, I., Eds.; Kluwer Academic Publishers: Dordrecht, 2002; p 111.
19. Bogatyreva, G. P.; Marinich, M. A.; Gvyazdovskaya, V. L. Diamond Relat Mater 2000, 9, 2002.
20. Dolmatov, V.; Shenderova, O.; Gruen, D., Eds. William-Andrew Publishing: Norwich, NY, 2006.
21. Dolmatov, V. Y. Russ Chem Rev 2001, 70, 607.
22. Hu, Y. H.; Shenderova, O. A.; Hu, Z.; Padgett, C. W.; Brenner, D. W. Reports Prog Phys 2006, 69, 1847.
23. Li, L.; Davidson, J. L.; Lukehart, C. M. Carbon 2006, 44, 2308.
24. Schreiner, P. R.; Fokina, N. A.; Tkachenko, B. A.; Hausmann, H.; Serafin, M.; Dahl, J. E. P.; Liu, S.; Carlson, R. M. K.; Forkin, A. A. J Org Chem 2006, 71, 6709.
25. Liu, Y.; Gu, Z.; Margrave, J. L.; Khabashesku, V. N. Chem Mater 2004, 16, 3924.
26. Liu, Y.; Khabashesku, V. N.; Halas, N. J. J Am Chem Soc 2005, 127, 3712.
27. Yang, J. H.; Song, K. S.; Zhang, G. J.; Degaw, M.; Sasaki, Y.; Ohdomari, I.; Kawarada, H. Langmuir 2006, 22, 11245.
28. Kossovsky, N.; Gelman, A.; Hnatyszyn, H. J.; Rajguru, S.; Garrell, R. L.; Torbati, S.; Freitas, S. S.; Chow, G. M. Bioconjugate Chem 1995, 6, 507.
29. Zhang, X. Q.; Chen, M.; Lam, R.; Xu, X. Y.; Osava, E.; Ho, D. ACS Nano 2009, 3, 2609.
30. Pu, H. T.; Liu, L.; Chang, Z. H.; Yuan, J. J. Electronchim Acta 2009, 54, 7536.
31. Chung, T. S. Plast Eng 1997, 41, 701.
32. Kasowski, R. V.; Lee, K. S. U.S. Patent 5,386,326, 1995.
33. Choe, E. W.; Choe, D. D. In Polybenzimidazoles; Salamone, J. C., Ed.; CRC Press: Boca Raton, FL, 1996; p 5619.
34. Sansone, M. J. U.S. Patent 4, 693,824, 1987.
35. Wainright, S.; Wang, J. T.; Weng, D.; Savinel, R. F.; Litt, M. H. J Electrochem Soc 1995, 142, L121.
36. Glipa, X.; Bonnet, B.; Mule, B.; Jones, D. J.; Roziere, J. J Mater Chem 1999, 9, 3045.
37. Choi, S. H.; Coronas, J.; Lai, Z. P.; Yust, D.; Onarato, F.; Tsapatsis, M. J Membr Sci 2008, 316, 145.
38. Baek, J. B.; Lyons, C. B.; Tan, L. S. Macromolecules 2004, 37, 8278.
39. Xu, H. J.; Chen, K. C.; Gao, X. X.; Fang, J. H.; Yin, J. Polymer 2007, 48, 5556.
40. Shao, H. Z.; Shi, Z. X.; Fang, J. H.; Yin, J. Polymer 2009, 50, 5987.
41. Zhao, B.; Hu, H.; Robert, C. H. Adv Funct Mater 2004, 14, 71.
42. Wang, D. H.; Tan, L. S.; Huang, H. J.; Dai, L. M.; Osawa, E. J. Macromolecules 2009, 42, 114.
43. Zeng, K.; Zheng, S. X. J Phys Chem B 2007, 111, 13919.
44. Beamson, G.; Briggs, D. Radiation Effects on Polymers for Biological Use; Wiley: Chichester, 1992.
45. Tamaki, R.; Choi, J.; Laine, R. M. Chem Mater 2003, 15, 793.
46. Choi, J.; Tamaki, R.; Kim, S. G.; Laine, R. M. Chem Mater 2003, 15, 3365.
47. Zhang, Q. X.; Naito, K.; Tanaka, Y.; Kagawa, Y. Macromol Rapid Commum 2007, 28, 2069.
48. Liu, H. Z.; Zheng, S. X.; Nie, K. Z. Macromolecules 2005, 38, 5088.
49. Liu, Y.; Shi, Z. X.; Xu, H. J.; Fang, J. H.; Ma, X. D.; Yin, J. Macromolecules 2010, 43, 6731.
50. Asunction, M. Z.; Laine, R. M. Macromolecules 2007, 40, 555.